

Aharonov-Casher Effect and the Coherent Flux Tunneling in the Hybrid Charge Quantum Interference Device

J. W. Dunstan and K. H. Kim

Royal Holloway, University of London, Egham Hill, Egham TW20 0EX, United Kingdom

R. Shaikhaidarov, A. Shesterikov, and I. Antonov

Royal Holloway, University of London, Egham Hill, Egham TW20 0EX, United Kingdom and

National Physical Laboratory, Hampton Road, Teddington, TW11 0LW, United Kingdom

S. Linzen and E. V. Il'ichev

Leibniz Institute of Photonic Technology, D-07702 Jena, Germany

V. N. Antonov and O. V. Astafiev

Royal Holloway University of London, Egham, Surrey, TW20 0EX, United Kingdom

By exploiting the Aharonov-Casher effect we demonstrate a suppression of magnetic flux tunneling in a Hybrid Charge Quantum Interference Device. The main part of this device is two Josephson junctions with a small superconducting island between them. To minimize phase fluctuations across Josephson junctions, this structure is embedded in a compact super-inductive NbN loop. The Interference between the flux tunneling paths is determined by the island-induced charge, which is controlled by an external voltage. The charge sensitive operation of the device is subjected to poisoning by the quasiparticles generated in the NbN film.

The Aharonov-Casher (AC) effect, the interference of fluxons around a static charge, is dual to the Aharonov-Bohm (AB) effect, the interference of the charged particles encircling a magnetic flux [1]. The AC effect in superconducting coherent circuits has been the subject of a few works so far. The effect was experimentally demonstrated in spectroscopy of the charge and bifluxon qubits [2, 3], switching current of the linear array of Josephson junctions (JJ) [4], and resistance of the JJ network [5]. Freedman and Averin suggested using the AC effect to completely suppress fluxon tunneling in the JJs [6]. Partially this has been achieved in bifluxon qubit [3] and Charge Quantum Interference Device (CQUID) [7]. In the latter experiment, the JJs were replaced with the nanowires. Despite a similar appearance in the experiment, the underlying physics of nanowires and JJs is somewhat different [7, 8]. In addition, complete suppression of the fluxon tunneling has not been demonstrated in both experiments.

To demonstrate AC effect, one has to ensure operation of JJs/nanowires in the regime of coherent quantum phase slip (CQPS). It requires screening the CQPS centre from the environmental noise, because the phase slip energy E_S is usually tiny, few μV (~ 30 - 50 mK). External noise engages phase fluctuations, thus further reducing E_S . In RF-SQUID-type devices, where phase fluctuation is also an issue, a large superconducting loop with high inductance is used [9]. In later work, high inductance was realized by a linear array of JJs. Alternatively, CQUID used an NbN film with extreme kinetic inductance ($L_{\square} \sim 1.6$ nH) as the material of the loop [7]. This made the device very compact and resistant to external flux noise.

However, there are limitations of the CQUID, which

has the nanowires as CQPS centres: the width of the nanowires required by the CQPS, ~ 10 nm, is at the limit of nanofabrication accuracy, which is currently about ± 2 nm. There is large variation in the CQPS energy E_S due to its exponential sensitivity to the width of nanowires [10–12]. In contrast, JJs can be fabricated with fairly good reproducibility of parameters, better than 90 %. Currently, JJs integrated with high inductance materials are an active field of research for the engineering of superconducting coherent circuits [3, 13, 14]. For example NbN, TiN, or InO_x wires replace the super-inductive array of JJs in the applications where a small stray capacitance is required [15–17].

In our work we designed the hybrid CQUID (h-CQUID), where the JJs are combined with the high kinetic inductance NbN films. The h-CQUID has the advantage of reliable control of the parameters compared to CQUID (the yield of the nanowires with proper parameters after fabrication is below 0.3), compactness of the high kinetic inductance material, and low stray capacitance.

Figure 1 displays SEM images of the sample and the experimental setup. In h-CQUID the JJs are embedded in the NbN loop. The NbN films grown by atomic layer deposition [18]. The JJs have good galvanic contact with the NbN loop.

As will be shown below, for such a structure the interference of fluxons crossing the JJs can be controlled by the gate voltage up to complete suppression of the fluxon tunnelling, thereby increasing the functionality of the h-CQUID, and confirming the theoretical prediction [6].

The Hamiltonian of the system in the flux basis can be

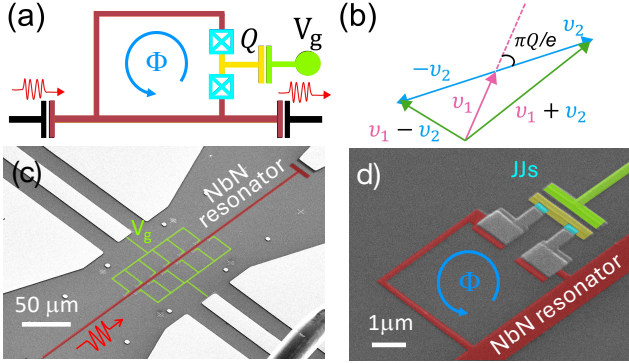


FIG. 1. (a) A schematic of the sample. The h-CQUD consists of the superconducting loop (venous) interrupted by two Josephson junctions (cyan). A superconducting island (yellow) between the junctions is capacitively coupled to a voltage gate. The h-CQUD shares part of the loop with $\lambda/2$ resonator. (b) A representation of addition and subtraction of phase slip phasors in Josephson junction 1 and 2. The angle between the phasors is $\pi Q/e$. With additional quasiparticle in the island, the total phase slip amplitude becomes $|v_1 - v_2|$. (c) The SEM image (false colour) of multiple h-CQUDs coupled to a $\lambda/2$ resonator (venous) and gate electrodes (green). (d) SEM image of a single h-CQUD. The picture has the same colour scheme as (a) and (c).

written as:

$$\hat{H} = -(\epsilon/2)\hat{\sigma}_z - (E_S/2)\hat{\sigma}_x \quad (1)$$

where $\epsilon = 2I_p\Delta\Phi$ is the energy difference between the two fluxon number states, E_S is the coupling energy between these states, and σ_z and σ_x are Pauli matrices. Here, $I_p = \Phi_0/2L_k$ is the persistent current, L_k the kinetic inductance of the loop, $\Delta\Phi = \Phi - (N + 1/2)\Phi_0$ is the deviation from the degeneracy point. The coupling energy E_S , also known as the phase slip energy, is related to the tunneling rates of the fluxons, $\nu_{1,2}$, across the JJs $E_S(Q) = \hbar|\nu_1 + e^{i2\pi Q}\nu_2|$. In the latter equation Q is the charge on a small Al island between the JJs. The charge is induced by the voltage V_g at the metal gate, $Q = C_g V_g$. It changes the vector sum of the fluxon tunneling rate, see Figure 1(b) for two values of Q , different by the charge of electron e [4, 7]. The excitation energy of the qubit is

$$\Delta E = \sqrt{\epsilon(\Phi)^2 + E_S(Q)^2} \quad (2)$$

It depends on both the external magnetic flux Φ as in a conventional RF-SQUID, and the induced charge Q .

The h-CQUD is inductively coupled to a line resonator. For probing of the qubit state, we used two-tone spectroscopy with a dispersive readout at the resonant frequency of the resonator. Five samples were measured. Each of them had four h-CQUDs coupled to the same resonator. The experimental data presented here are taken from one of the samples. Measurements were performed at 12 mK in a dilution refrigerator.

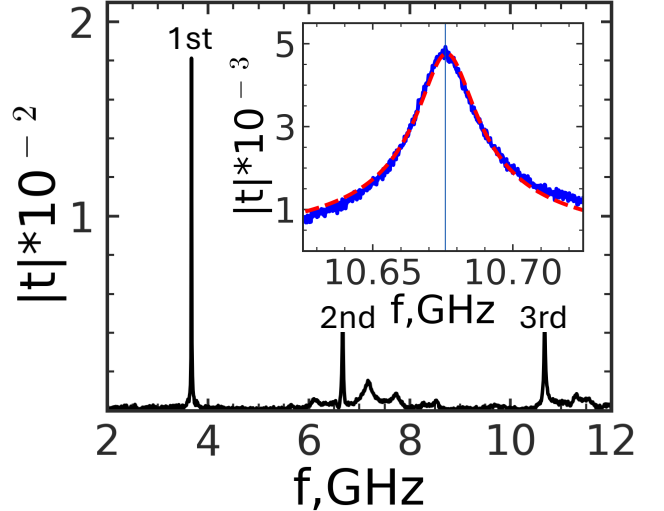


FIG. 2. Transmission of the NbN line resonator. There are 3 resonance modes in the spectral range of our measurement: 3.671 GHz, 6.670 GHz, 10.676 GHz. Insert: Third mode (blue) at 10.676 GHz is used for two-tone spectroscopy. Dashed red line is the Lorentzian fit. The resonance has a quality factor of $Q \approx 520$.

We probe transmission through the resonator with the Vector Network Analyser (VNA). The input microwave line has -83 dB attenuation from room to low temperature. The transmitted signal is amplified by $+35$ dB at low temperature and $+35$ dB at room temperature before reaching the VNA input port. There are three modes of the resonator in the experimental range see Fig. 2. Ideally, they should be equidistant with frequencies $f_n = nv/2L$ ($n=1, 2, 3$, v is the phase velocity, and L is the length of the resonator, v is the phase velocity). In experiment resonance frequencies usually deviates from the calculated values, because of the qubit loops inductively coupled to the resonator. For two-tone spectroscopy we use 3rd resonance at 10.676 GHz. It has a quality factor $Q \approx 520$. Despite the quality factor of this resonance concedes to that of 1st and 2nd modes, it has the strongest coupling to the h-CQUD under analysis.

Figure 3(a) shows a two-tone spectroscopy of the sample: we probe transmission of the resonator at 10.676 GHz while sweeping the second MW signal from 0.1 GHz to 10 GHz. The transmission drops when the frequency of the second MW signal is equal to the excitation frequency of the qubit, $\Delta E/h$. The frequency scans at different magnetic fluxes are compiled in the intensity plot. We focus on the spectral line of the flux qubit positioned in the centre. The minimum of this spectral line at the degeneracy point $\Delta\Phi=0$ is, $f = 2.555$ GHz. We fit the curve with (2) and find a persistent current of the loop $I_p \sim 11.5$ nA. It corresponds to the total inductance of the h-CQUD loop with the JJs of 90 nH. There are few additional spectroscopy lines of different nature, which are not important for our analysis: other reso-

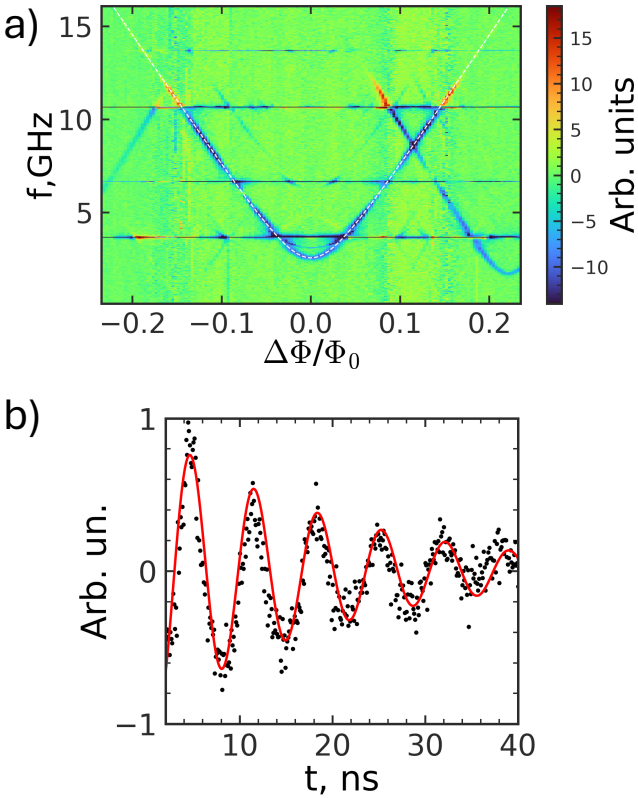


FIG. 3. (a) Two-tone spectroscopy of the h-CQUID at different deviation of magnetic flux $\Delta\Phi$ from the degeneracy point. The spectral line is overlaid with white dashed line of equation (2). The parameters of the fit line are: $I_p = 11.5$ nA, $E_S(Q) = 2.555$ GHz. There are additional spectroscopy lines in the intensity plot (the modes of resonator, different qubits etc.) (b) Rabi oscillations of the qubit taken at the degeneracy point $\Delta\Phi=0$. The relaxation time of qubit $T_1=20$ ns.

nances of the sample, the modes of the linear resonator, and higher excitations of the structure under study. The Rabi oscillations of the h-CQUID taken at the degeneracy point $\Delta\Phi=0$ are shown in Fig. 3(b). From the fit of the oscillations we find the relaxation time $T_1 \simeq 20$ ns. It is much smaller than in the modern qubit, where T_1 reaches millisecond. Partially, such a low relaxation time can be attributed to a strong inductive coupling of the h-CQUID loop to the resonator.

There is an additional gate voltage control of the h-CQUID. We fix the magnetic flux at the degeneracy point and compile the frequency scans at different V_g to the intensity plot of Fig. 4(a). There are two spectral lines that oscillate with period $Q = 2e$. The oscillation phase of them is exactly shifted by e . The effect is similar to that seen in CQUID with superconducting nanowires replacing the JJs [7]. The oscillations are manifestations of the Aharonov-Casher effect. Near the point of destructive interference, $Q = 2e(n + 1/2)$, the flux tunneling rate ν should be minimal. In the ideal case of two identical JJs, when $\nu_1 = \nu_2$, the flux tunneling should be

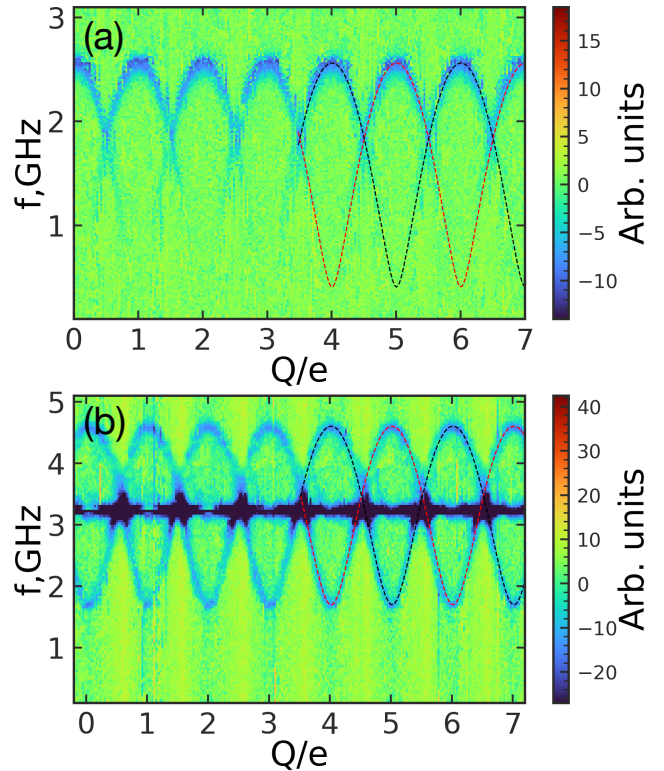


FIG. 4. (a) Spectroscopy of the h-CQUID under study at the degeneracy point $\Delta\Phi=0$ taken at different $Q = C_g V_g$. h-CQUID has small asymmetry of JJs, $\nu_1 = 1.48$ GHz and $\nu_2 = 1.08$ GHz. There are two oscillating curves with even and odd parities of charge. The period of oscillations of individual curve is $2e$. The curves are overlaid with the dashed fitting lines of Eq. 2. (b) Spectroscopy of the h-CQUID with large asymmetry of JJs, $\nu_1 = 3.15$ GHz and $\nu_2 = 1.45$ GHz.

completely suppressed, the excitation energy of the qubit should tend to zero, and the spectral lines should vanish [6]. We fit experimental curves with $\nu = |\nu_1 \pm \nu_2 e^{i2\pi Q}|$, with $\nu_1 = 1.48$ GHz and $\nu_2 = 1.08$ GHz. The minimum of $E_S/h \approx 0.4$ GHz corresponds to the case when two phase slip phasors have opposite directions. The different tunneling rates are a consequence of different parameters of the JJ in h-CQUID. We discuss this in the following section. The presence of two spectroscopy curves in Fig. 4 is a sign of the quasi-particle poisoning of the Al island between the JJs. We believe that these unpaired electrons are excited by the microwave noise in the highly inductive NbN loop [7]. Quasi-particle poisoning presents a serious problem for the devices utilizing superconducting films of high kinetic inductance [16].

In small JJ with E_J few times larger than E_C the tunneling rate of the fluxons can be found from

$$\nu = \frac{8}{\hbar} \sqrt{E_J E_C / \pi} (8E_J/E_C)^{1/4} \exp(-\sqrt{8E_J/E_C}) \quad (3)$$

where $E_C = e^2/2C$, $E_J = R_q \Delta/2R_N$, and R_N are the charging energy, the Josephson energy, and the nor-

mal resistance [19, 20]. We estimate $E_C/h \approx 13.8$ GHz and $E_J/h \approx 29.2$ GHz using the specific capacitance $\sim 5 \times 10^{-16}$ F/ μm^2 , junction area $0.28 \times 0.1 \mu\text{m}^2$, $\Delta_{Al}=202$ μV , and $R_N = 5.0$ k Ω [21]. Then the fluxon tunneling rate from equation (3) is $\nu \approx 2.7$ GHz. It is twice larger than the experimentally found 1.48 GHz and 1.08 GHz. Poor agreement can be explained by exponential sensitivities of ν to the parameters of the JJ tunnel barrier. The tunneling barrier affects the Josephson energy in a large way compared to the charging energy. The charging energy E_C is determined more steadily from the geometry of the JJ. An uncertainty of less than 5 % can be expected. To be close to the experimental value, the ratio E_J/E_C should be in the range of 3.0-3.2 (we fix $E_C = 13.8$ GHz) compared to ~ 2.3 in our calculation. The strong sensitivity of E_J to the fabrication process explains the 40 % difference between geometrically identical ν_1 and ν_2 . To demonstrate effect of asymmetry of the JJ we show the spectroscopy curve of h-CQUID, where the tunnelling rates are quite different, $\nu_1 = 3.15$ GHz and $\nu_2 = 1.45$ GHz, see Fig. 4(b). The overlapping areas of the JJs in this sample are only slightly different, their ratio is 2.5/2. One can clearly see the top and the bottom of the spectroscopy curves.

So far we have discussed h-CQUID using CQPS model of the JJs. It is also instructive to model h-CQUID starting from the flux qubit Hamiltonian in the basis of superconducting phase. The Hamiltonian of the superconducting loop with two identical Josephson junctions reads

$$H = -8E_C \partial^2 / \partial \phi^2 - 2E_J |\cos(\phi/2)| + \frac{E_L}{2} (\phi - \phi_{ext})^2 \quad (4)$$

where $E_L = \Phi_0^2 / 4\pi^2 L_k$, ϕ is the total superconducting phase difference of the two junctions, $\phi = \phi_1 + \phi_2$, and $\phi_{ext} = 2\pi\Phi_{ext}/\Phi_0$ [22]. Note that E_C and E_J are taken for a single junction, so that both the kinetic and Josephson energy terms in the Hamiltonian are approximately doubled compared to usual RF-SQUID [23, 24]. Also the

Hamiltonian (4) assumes a well-defined phase and does not include the effect of single electron charging of the island. Therefore, we fit only the spectroscopy line in Fig. 3(b). The produce the best fit using the numerical diagonalization of the Hamiltonian (4) and varying E_J and E_L (E_C is again fixed to 13.8 GHz). The simulation gives $E_J/h = 27.9$ GHz, $E_L/h = 1.89$ GHz ($L_k=81.3$ nH). Despite the simplicity of this model, these parameters are consistently close to the values obtained from the fit of the curves with equation (2).

In conclusion, we demonstrate operation of hybrid CQUID, made of a combination of high inductive NbN loop and JJs. The yield of such h-CQUID is substantially higher than that of the CQUID made of the superconducting nanowires. The fluxons coherently tunneling through the small Josephson junctions develop interference, which is controlled with the charge induced at the island between the JJs (Aharonov-Casher effect). When the induced charge has an odd number of electron charges e , the interference is destructive so that the flux tunneling rate tends to zero. It is seen as a dissolution of the spectroscopy line of the h-CQUID. Although h-CQUID has better control of the fluxon tunneling rate compared to original CQUID, it does not eliminate the problem of quasiparticles poisoning of the device. The latter has its origin in the quasiparticle excitations in the NbN film under the MW signal.

This work was supported by EMPIR 20FUN07 SuperQuant, and UK Engineering and Physical Sciences Research Council (EPSRC) Grant No. EP/Y022637/1. S.L and E.I would like to thank the German Federal Ministry of Research, Technology and Space (BMFTR) for partial support under Grant No. 13N17121/NbNanoQ.

DATA AVAILABILITY

The data generated in this study have been deposited in the Open Science Framework repository. They can be obtained without any restriction at <https://osf.io/Q4dav>.

[1] Y. Aharonov and A. Casher. Topological quantum effects for neutral particles. *Phys. Rev. Lett.*, 53:319–321, Jul 1984.

[2] M. T. Bell, W. Zhang, L. B. Ioffe, and M. E. Gershenson. Spectroscopic evidence of the aharonov-casher effect in a cooper pair box. *Phys. Rev. Lett.*, 116:107002, Mar 2016.

[3] K. Kalashnikov, W.T. Hsieh, W. Zhang, W.-S. Lu, P. Kamenov, A. Di Paolo, A. Blais, M.E. Gershenson, and M. Bell. Bifluxon: Fluxon-parity-protected superconducting qubit. *Phys. Rev. X Quantum*, 1:010307, 2020.

[4] I. M. Pop, B. Douçot, L. Ioffe, I. Protopopov, F. Lecocq, I. Matei, O. Buisson, and W. Guichard. Experimental demonstration of aharonov-casher interference in a josephson junction circuit. *Phys. Rev. B*, 85:094503, Mar 2012.

[5] W. J. Elion, J. J. Wachters, L. L. Sohn, and J. E. Mooij. Observation of the aharonov-casher effect for vortices in josephson-junction arrays. *Phys. Rev. Lett.*, 71:2311–2314, Oct 1993.

[6] J.R. Friedman and D. V. Averin. Aharonov-casher-effect suppression of macroscopic tunneling of magnetic flux. *Phys. Rev. Lett.*, 88:050403, Jan 2002.

[7] S. E. de Graaf, S. T. Skacel, T. Höngl-Decrinis, R. Shaikhaidarov, H. Rotzinger, S. Linzen, M. Ziegler, U. Hübner, H.-G. Meyer, V. Antonov, E. Il'ichev, A. V. Ustinov, A. Ya. Tzalenchuk, and O. V. Astafiev. Charge quantum interference device. *Nature Physics*, 14(6):590–594, Jun 2018.

[8] S. E. de Graaf. Dual fraunhofer interference and charge fluctuations in long quantum phase slip wires. *Phys. Rev. B*, 102:144509, Oct 2020.

[9] E. Il'ichev, V. Zakosarenko, R.P.J. IJsselsteijn, and Schulze. V. Inductive reply of high- T_c rf squid in the presence of large thermal fluctuations. *J Low Temp Phys*, 106:503–508, 1997.

[10] J. T. Peltonen, O. V. Astafiev, Yu. P. Korneeva, B. M. Voronov, A. A. Korneev, I. M. Charaev, A. V. Semenov, G. N. Golt'sman, L. B. Ioffe, T. M. Klapwijk, and J. S. Tsai. Coherent flux tunneling through nbn nanowires. *Phys. Rev. B*, 88:220506, Dec 2013.

[11] D.S. Golubev and A.D. Zaikin. Quantum tunneling of the order parameter in superconducting nanowires. *Phys. Rev. B*, 64:014504, Jun 2001.

[12] A.D. Zaikin, D.S. Golubev, A. van Otterlo, and G.T. Zimányi. Quantum phase slips and transport in ultrathin superconducting wires. *Phys. Rev. Lett.*, 78:1552–1555, Feb 1997.

[13] V.E. Manucharyan, J. Koch, L.I. Glazman, and M.H. Devoret. Fluxonium: single cooper-pair circuit free of charge offsets. *Science*, 326(5949):113–116, 2009.

[14] I.V. Pechenezhskiy, R.A. Mencia, L.B. Nguyen, Y.-H. Lin, and V.E. Manucharyan. The superconducting quasicharge qubit. *Nature*, 585:368–371, 09 2020.

[15] R.S. Shaikhdarov, Kyung Ho Kim, Jacob W. Dunstan, I.V. Antonov, S. Linzen, M. Ziegler, Dmitry S. Golubev, V. N. Antonov, E. V. Il'ichev, and O. V. Astafiev. Quantized current steps due to the a.c. coherent quantum phase-slip effect. *Nature*, 608(7921):45–49, Aug 2022.

[16] R.S. Shaikhdarov, K.H. Kim, J. Dunstan, I. Antonov, D. Golubev, V.N. Antonov, and O.V. Astafiev. Quantized current steps due to the synchronization of microwaves with bloch oscillations in small josephson junctions. *Nature Communications*, 15(1):9326, 2024.

[17] R.S. Shaikhdarov, I. Antonov, K.H. Kim, A. Sheslerikov, S. Linzen, E.V. Il'ichev, V.N. Antonov, and O.V. Astafiev. Feasibility of the Josephson voltage and current standards on a single chip. *Applied Physics Letters*, 125(12):122602, 09 2024.

[18] S Linzen, M Ziegler, O V Astafiev, M Schmelz, U Hübner, M Diegel, E Il'ichev, and H-G Meyer. Structural and electrical properties of ultrathin niobium nitride films grown by atomic layer deposition. *Superconductor Science and Technology*, 30(3):035010, jan 2017.

[19] G. Schön and A. D. Zaikin. Quantum coherent effects, phase transitions, and the dissipative dynamics of ultra small tunnel junctions. *Physics Reports*, 198(5):237–412, 1990.

[20] D. V. Averin, A. B. Zorin, and K. K. Likharev. Bloch oscillations in small josephson junctions. *Sov. Phys. JETP*, 61, 1985.

[21] F. Deppe, S. Saito, H. Tanaka, and H. Takayanagi. Determination of the capacitance of nm scale josephson junctions. *Journal of Applied Physics*, 95(5):2607–2613, 2004.

[22] V. I. Shnyrkov, A. A. Soroka, and S. I. Melnyk. The two-josephson-junction flux qubit with large tunneling amplitude. *Low Temperature Physics*, 34:610–616, Aug 2008.

[23] A. Yu. Dmitriev and O. V. Astafiev. A perspective on superconducting flux qubits. *Applied Physics Letters*, 119(8):080501, 08 2021.

[24] J. T. Peltonen, P. C. J. J. Coumou, Z. H. Peng, T. M. Klapwijk, J. S. Tsai, and O. V. Astafiev. Hybrid rf squid qubit based on high kinetic inductance. *Scientific Reports*, 8(1):10033, Jul 2018.